International Journal of Nanomedicine

Dovepress
open access to scientific and medical research

Open Access Full Text Article

ORIGINAL RESEARCH

Microwave-assisted green synthesis of superparamagnetic nanoparticles using fruit peel extracts: surface engineering, T_2 relaxometry, and photodynamic treatment potential

This article was published in the following Dove Press journal:
International Journal of Nanomedicine
10 August 2016
Number of times this article has been viewed

Shazia Bano[1–3]
Samina Nazir[2]
Alia Nazir[1]
Saeeda Munir[3]
Tariq Mahmood[2]
Muhammad Afzal[1]
Farzana Latif Ansari[4]
Kehkashan Mazhar[3]

[1]Department of Physics, The Islamia University of Bahawalpur, Bahawalpur, [2]Nanosciences and Technology Department, National Centre for Physics, [3]Institute of Biomedical and Genetic Engineering (IBGE), [4]Pakistan Council for Science and Technology, Islamabad, Pakistan

Abstract: Superparamagnetic iron oxide nanoparticles (SPIONs) have the potential to be used as multimodal imaging and cancer therapy agents due to their excellent magnetism and ability to generate reactive oxygen species when exposed to light. We report the synthesis of highly biocompatible SPIONs through a facile green approach using fruit peel extracts as the biogenic reductant. This green synthesis protocol involves the stabilization of SPIONs through coordination of different phytochemicals. The SPIONs were functionalized with polyethylene glycol (PEG)-6000 and succinic acid and were extensively characterized by X-ray diffraction analysis, field emission scanning electron microscopy, energy-dispersive X-ray spectroscopy, atomic force microscopy, Rutherford backscattering spectrometry, diffused reflectance spectroscopy, fluorescence emission, Fourier-transform infrared spectroscopy, ultraviolet-visible spectroscopy, and magnetization analysis. The developed SPIONs were found to be stable, almost spherical with a size range of 17–25 nm. They exhibited excellent water dispersibility, colloidal stability, and relatively high R_2 relaxivity (225 mM^{-1} s^{-1}). Cell viability assay data revealed that PEGylation or carboxylation appears to significantly shield the surface of the particles but does not lead to improved cytocompatibility. A highly significant increase of reactive oxygen species in light-exposed samples was found to play an important role in the photokilling of human cervical epithelial malignant carcinoma (HeLa) cells. The bio-SPIONs developed are highly favorable for various biomedical applications without risking interference from potentially toxic reagents.

Keywords: green approach, biocompatible, multifunctional, bio synthesis, surface modification, microwave incubation, MRI contrast agent, photosensitive SPIONs

Introduction

Superparamagnetic iron oxide nanoparticles (SPIONs) have been the subject of intensive research due to their excellent magnetism and the hydrophilic surface that can be modified for long circulation times.[1–4] In the nanometer range, they are considered suitable candidates for biomedical applications, such as photodynamic therapy (PDT), magnetic resonance imaging (MRI), drug delivery, and hyperthermia.[5,6] To be successfully utilized for biomedical applications, it is essential to develop narrow-sized magnetite with biocompatible surface to render SPIONs nonimmunogenic and nonantigenic, as well as to reduce their interaction with plasma proteins such as formation of "corona".[7]

Correspondence: Samina Nazir
Nanosciences and Technology Department, National Centre for Physics, Islamabad 44000, Pakistan
Tel +92 302 850 5080
Email seegasami01@yahoo.com

submit your manuscript | www.dovepress.com
Dovepress
http://dx.doi.org/10.2147/IJN.S106553

Chemical approaches usually involve the use of potentially toxic reactants, which may result in environmental and biological risks.[8–10] Moreover, these processes mostly end up with hydrophobic nanoparticles (NPs), which are often subjected to surface engineering, making them water dispersible.[11–13] The absorption of NPs produced by hydrophobic polymers is greater than that of NPs produced by hydrophilic polymers.[14,15] However, hydrophobic NPs may induce genotoxicity, carcinogenicity, and teratogenicity; therefore, a hydrophilic surface is preferred over the hydrophobic surface for biomedical applications.[16–19]

Consequently, numerous efforts have been focused on refining the properties of metal NPs through modification of their synthesis methods from conventional methods to green ones. Some of these include the use of seaweed,[20] tea,[21,22] as well as peel extracts of plantain,[23] banana,[24] and orange.[25] Although biocompatibility has been achieved in such reports, there is a dire need for the successful surface engineering of such biologically safer NPs to enable a variety of biomedical and other industrial applications.

We have developed a microwave (MW)-assisted green route resulting in biocompatible and stable multifunctional SPIONs suitable for biomedical applications. This is a one-pot green protocol in which MW irradiation leads to the successful formation of SPIONs from iron chloride, while phytochemicals from fruit peel extracts serve as bioreductants. Natural products such as polysaccharides, polyphenols, proteins, amino acids, vitamins, and organic acids from plants are useful in reduction and surface capping of NPs.[26–29]

The principal objective of this work was to develop a simple but efficient route for the synthesis and functionalization of biologically safer SPIONs for biomedical applications. It was hypothesized that the use of MW heating may reduce the reaction time by many orders of magnitude.[30–32] We also developed a simple one-pot MW incubation protocol for the attachment of polyethylene glycol (PEGylation) and acidification of bio-SPIONs and compared our results with the conventionally used linker-aided procedure using carbodiimide chemistry. The biocompatibility and T_2 relaxivity of the formed pristine and functionalized SPIONs were investigated against those of human cervical epithelial malignant carcinoma (HeLa) cells.

Recently, use of metal-based photoactive NPs has emerged as a successful strategy for PDT.[33,34] The nontoxic and hydrophilic metal NPs could improve solubility issues and enhance tumor targeting due to the higher penetration and retention effects.[33,34] Hence, we also investigated and report herein the photooxidative capability of bio-SPIONs relative to HeLa cells.

Materials and methods

Unless otherwise stated, all reagents were obtained from Sigma-Aldrich Co. (St Louis, MO, USA). Ferric chloride tetra hydrate ($FeCl_3 \cdot 4H_2O$, 97%), PEG-6000, succinic anhydride (SA) >99%, sulforhodamine B (SRB), trichloroacetic acid, 3-(4,5-dimethylthiazol-2-yl)-2,5-diphenyltetrazolium bromide (MTT), 1,3-diphenylisobenzofuran, thiobarbituric acid (TBA), and sodium azide (NaN_3) were used in this study.

Preparation of peel extracts

Citrus aurantium (orange), *Punica granatum* (pomegranate), *Malus domestica* (apple), and *Citrus limon* (lemon) were first rinsed thoroughly using Milli-Q water. Using a paring knife, segments of colored peel were carefully cut away from the fruit and then further cut into small pieces. A small quantity (25 g) of thoroughly washed and finely chopped (length: 0.5±0.03 cm; thickness: 2–3±0.05 mm [apple and lemon] and 5–6±0.02 mm [orange and pomegranate]) peels were sonicated in 250 mL of double distilled water for 10 minutes and boiled at 100°C for 3 hours with stirring. The colored extract was filtered through a Whatman® Grade 2 (pore size: 8 µm) qualitative filter paper (Sigma-Aldrich Co., St Louis, MO, USA).

Aqueous peel extracts were also prepared via MW irradiation. The same quantity (25 g) of thoroughly washed, finely chopped peels was kept in 250 mL of Milli-Q water for 20 minutes and heated for 5 minutes under MW irradiation (Dawlance, 800 W; Dawlance Private Ltd, Karachi, Pakistan). The colored extract was centrifuged at 4,000 rpm for 3 minutes and stored at 4°C.

Biosynthesis of iron oxide NPs

$FeCl_3 \cdot 4H_2O$ (2 mmol) was dissolved in 10 mL of Milli-Q water in a reaction flask. A 25 mL aliquot of peel extract was added, and the clear solution obtained was subjected to MW (Dawlance, 800 W) irradiation (30-second impulses). The appearance of black color indicated the formation of iron oxide NPs (IONPs). The nanofluids were centrifuged (4,000 rpm, 30 minutes), and the precipitates were washed with Milli-Q water several times to remove excess phytochemicals. Fruit peel extracts from pomegranate, lemon, orange, and apple yielded four types of biologically reduced SPIONs: pomegranate peel-mediated SPIONs (PP-SPIONs), lemon peel-mediated SPIONs (LP-SPIONs), orange peel-mediated SPIONs (OP-SPIONs), and apple peel-mediated SPIONs (AP-SPIONs), respectively.

In order to compare the biocompatibility of bio-SPIONS with chemically synthesized IONPs, magnetite NPs were prepared via the chemical coprecipitation method (Supplementary materials).

Surface engineering through carbodiimide chemistry

Bio-SPIONs were functionalized using carbodiimide chemistry following literature with some modification.[35] Briefly, equal amounts of 1-ethyl-3-(3-dimethylaminopropyl)carbodiimide (EDC) and PEG-6000 (or SA) were added into 5 mL dimethyl sulfoxide, and the solution was stirred for 3 hours. Bio-SPIONs were added to the activated linker (PEG or SA) and stirred continuously for 48 hours. Functionalized SPIONs were dialyzed for 4 hours against Milli-Q water with Spectra/Por 6 Spectrum® (Spectrum Laboratories Inc., Rancho Dominguez, CA, USA) dialysis membrane (Spectrum Laboratories Inc., Rancho Dominguez, CA, USA); molecular weight cutoff: 25 kDa for removing the unbound linker and side products.

Surface engineering through MW incubation

Aqueous solutions of SPIONs were added to the activated linker (PEG or SA) and subjected to MW heating for 1 minute. Functionalized SPIONs were dialyzed for 4 hours against Milli-Q water with Spectra/Por 6 dialysis membrane (Spectrum Laboratories; molecular weight cutoff: 25 kDa) to remove the unbound linker.

PEG- and SA-modified samples, in subsequent discussions of this study, are designated as PEG-PP-SPIONs, PEG-LP-SPIONs, PEG-OP-SPIONs, PEG-AP-SPIONs, SA-PP-SPIONs, SA-LP-SPIONs, SA-OP-SPIONs, and SA-AP-SPIONs.

Characterizations

Ultraviolet (UV)-visible (vis) spectra were collected on an UV-vis Lambda 25 spectrophotometer (PerkinElmer Inc., Waltham, MA, USA). Photoluminescence spectra were obtained on LS 55 photoluminescence spectrometer (PerkinElmer Inc.) using a xenon lamp as the excitation source at room temperature. Diffuse reflectance spectra (DRS) of the SPIONs were obtained on a UV-vis/near-infrared (NIR) spectrometer (Lambda 950; PerkinElmer Inc.) with an integrating sphere of 900–2,500 nm range.

X-ray diffraction was performed on a D8 Advance X-ray diffractometer (Bruker Corporation, Billerica, MA, USA) with Cu Kα radiations (λ=1.54056 Å) at 45 kV energy and then analyzed.

The elemental composition of the SPIONs was evaluated through Rutherford backscattering spectroscopy. SPION powders were pelleted and were evaluated on a 5 MV Pelletron tandem accelerator using a He^{++} beam of energy 2.085 MeV operating at a 26 nA current density. A solid state barrier detector was used to evaluate the backscattering ions set at energy 20 keV.

Fourier transform infrared (FTIR) spectra were recorded using a Tensor 27 ATR ZnSe FTIR spectrometer (Bruker Corporation). Scanning electron micrographs were obtained using field emission scanning electron microscopy (FESEM) (Mira 3 XMU [1.2 nm]; Tescan Orsay Holding, a.s, Brno – Kohoutovice, Czech Republic) equipped with an energy-dispersive X-ray spectroscopy detector. The samples were carbon-coated prior to analysis. However, topographical images were obtained by atomic force microscopy (AFM) with an Agilent 5500 instrument operated at tapping mode.

The hydrodynamic diameter was measured with a Zetasizer (Nano ZSP; Malvern Instruments, Malvern, UK).

Magnetic measurements were carried out using a vibrating sample magnetometer (7407 VSM; Lake-Shore Cryotronics, Westerville, OH, USA).

MR relaxometry measurements

For the relaxivity measurements, different concentrations of SPIONs in 3% agarose gel were placed in microfuge tubes for imaging. T2-weighted images were obtained on an MR scanner (Achieva Intera 1.5T A-series; Philips Medical Systems, Best, the Netherlands) following the parameters repetition time (TR) =4,000 ms and echo time (TE) =50 ms. Images were analyzed using DICOM software (Philips Dicom Viewer R1.1V1L1-SP01; Philips Medical Systems) and at the Precision Work Station (670 series; software version R5.1V1L1SP1; Philips Medical Systems). Transverse relaxivity (R_2) was determined from the slope of the plot of 1/T2 against the metal concentration [Fe] in millimoles, using the Origin Pro 8 software (Originlab Corporation, Wellesley Hills, MA, USA).

Improvement of biocompatibility

Blood aggregation and hemolytic studies

Fresh human whole blood from a healthy volunteer donor was stabilized with heparin. Serum was removed from the blood sample and erythrocytes were collected by centrifugation at 2,000 rpm. The pellet was washed successively five times with phosphate-buffered saline (PBS) and then diluted ten times with the same solution after the last wash. Each of the test samples of ferric ions (concentration: 400 μg/mL) prepared

with PBS was added to the erythrocytes and incubated at 37°C for 2 hours. Double-distilled water and NaCl (0.1 M) were used as the positive and negative controls, respectively. A microplate reader (Thermo Fisher Scientific, Waltham, MA, USA) measured the absorbance of the leaked hemoglobin at 570 nm, with the absorbance at 620 nm as a reference, and the hemolysis percentage was calculated from the absorbance data after subtracting the background absorbance.

$$\% \text{ hemolysis} = \frac{A_S - A_{NC}}{A_{PC} - A_{NC}} \times 100 \quad (1)$$

where A_S is the absorbance of the sample, A_{NC} is the absorbance of the negative control, and A_{PC} stands for the positive control. The study was approved by the Research Ethical Committee of "Institute of Biomedical and Genetic Engineering (IBGE)", Islamabad. Doners written consent was obtained.

Cell viability determination using SRB assay

HeLa cells were obtained from the American Type Culture Collection (Manassas, VA, USA). Cell culture was maintained in modified medium (Supplementary materials).

In vitro cytotoxicity of SPIONs was measured using the SRB assay following a previous method with some modifications (Supplementary materials).[36]

Measurement of photokilling effect using MTT assay

To examine the photokilling effect, cells were irradiated using a 100 W tungsten light with an infrared filter for 5 minutes. After exposure, the cells were incubated for another 48 hours. Cell viability (CV) was measured by the MTT assay as described previously.[37] Absorbance was measured on a microplate reader (AMP PLATOS R-496) at the wavelength of 565 nm. Percentage viability was measured by subtracting the noncellular background from samples relative to the nontreated cells (NTCs) as negative control using the following formula:

$$\frac{OD_{treated}}{OD_{control}} \times 100 \quad (2)$$

Intracellular reactive oxygen species production

For the identification of possible reactive oxygen species (ROS) produced, HeLa cells were pretreated with sodium azide (NaN_3; 50 mM) and mannitol (1 mM) solution mixed in PBS and incubated for 1 hour, followed by photoirradiation and ROS analysis. Of the three groups, sodium azide (NaN_3) was added to the first group, mannitol to the second, and a combination of both NaN_3 and mannitol to the third group. In the fourth group, cells were exposed to both NaN_3 and mannitol without any SPIONs to detect any inhibitory effect of these scavengers. In the last group, HeLa cells were treated with NPs without any scavenger and incubated as described earlier. CV was measured by the MTT assay as described previously.

Induction of oxidative stress

Lipid peroxidation (LPO) level was quantified by the TBA reaction by measuring the formation of malondialdehyde (MDA). This method was used to measure spectrophotometrically the color produced by the reaction of TBA with MDA at 532 nm. MDA is one of the products of membrane LPO. Briefly, preseeded cultures were exposed to NPs for 24 hours. After the treatment, cells were washed and harvested in ice-cold PBS at 4°C. Cells were then lysed and centrifuged at 15,000× *g* for 10 minutes at 4°C. To the cell lysate, an equal amount of 10% sodium dodecyl sulfate was added, and the samples were incubated at room temperature for 5 minutes. Then, 0.25 mL of TBA (5.2 mg/mL) was added to the mixture and incubated at 95°C for 45 minutes. Absorbance of the mixture was measured at 532 nm using the NanoDrop 2000 (Thermo Fisher Scientific). All experiments were performed three times, with triplicates for each sample.

Data processing and statistics

Statistical analysis was conducted using SPSS 19 software (IBM Corporation, Armonk, NY, USA) and statistical comparisons were analyzed using one-way analysis of variance; two-tailed *t*-tests were used to investigate the differences between NTC, NP-treated, and solvent-exposed samples. In all cases, $P<0.05$ was considered significant.

Results and discussion

The development of biocompatible, reliable, and ecofriendly green routes for the fabrication of multifunctional NPs is of utmost importance to expand their biomedical applications.[38] SPIONs have already been synthesized via the green route by various investigators.[20–24,39,40] However, use of peel biomass has not been reported for the MW-assisted green synthesis of SPIONs with a narrow size distribution, increased stability, and multifunctionality, crucial for biokinetics and biodistribution in developing theranostics. The scheme of this work is described in Figure 1.

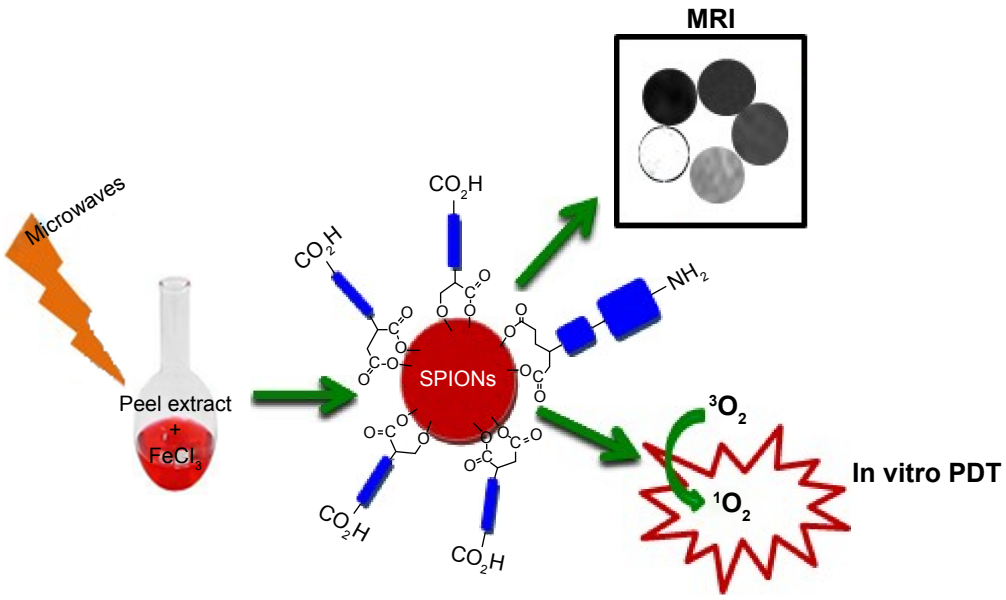

Figure 1 Schematic diagram of the work.
Abbreviations: MRI, magnetic resonance imaging; PDT, photodynamic therapy; SPIONs, superparamagnetic iron oxide nanoparticles.

Biosynthesis and characterization of SPIONs

This work focused on the production of SPIONs using peel extracts of four seasonal fruits. Peels of pomegranate, lemon, orange, and apple are the major sources of vitamins C and A,[10] whereas pomegranate peels contain antioxidants, especially polyphenols.[41,42] Using fruit waste as a cheaper bioreductant is a fascinating, simple, and green approach.[41,43]

Synthesis of SPIONs ensued when the aqueous fruit peel extract was mixed with the ferric chloride solution and heated under MW for 150 seconds. The reaction was monitored through UV-vis spectroscopy analysis after every 30 seconds. Once the reaction mixture became cool, it was subjected to optical studies.

Aqueous peel extracts were also prepared via MW irradiation. No difference was found in the UV-vis spectra of the peel extracts prepared by the two methods, and use of MW heating assisted us in avoiding the long conventional heating and resulted in the quick synthesis of SPIONs within a few minutes.

UV-vis spectroscopy

UV-vis spectra (Figure S1A) revealed that pomegranate peel extract was able to give slightly rod-shaped SPIONs under 30–60 seconds MW irradiation as indicated by their tailed absorption peak. However, after 150 seconds of MW heating it was giving two absorption peaks showing the elongated or dumbbell morphology of resulting PP-SPIONs. Such morphology arises from coupling between the electron clouds on NPs surface under the incident electromagnetic radiation.[44]

Similarly lemon and apple peel extracts lead to almost circular SPIONs even after 30 seconds MW heating. However, orange peels extract lead to slightly elongated SPIONs (Figure S1C) in a high yield after 120 seconds of MW heating.

Figure S2 shows broad absorbance for peel extracts especially for lemon and apple peels. Broad absorbance peak may likely result from various capping agents coming from different natural compounds.[10,27,29,42,45] The proceeding reaction could be envisioned via color changes in the resulting colloidal solution. Phytochemicals bound to the surface of bio- SPIONs are rich in hydrophilic hydroxyl groups that allowed the NPs to disperse and distribute homogenously in aqueous media (Table S1).[27–29, 42–45]

The major compounds found in apple peel extract are highly branched alcohols and aldehydes.[27] Several aldehydes and alcohols are also present in lemon and orange peel extracts.[29] Similarly, common phytochemical constituents in pomegranate peel extracts are glycerin, hydroxymethylfurfurole, guanosine and pyrogallol.[42–45] This higher abundances of multifunctional compounds in these peel extracts may be responsible for the synthesis of NPs.

X-ray diffraction and Rutherford backscattering spectroscopy

X-ray diffraction analysis of air-dried SPIONs confirmed the compositional consistency of the NPs (Figure 2A).

The observed lattice spacings at 30.3°, 35.8°, 37.4°, 43.3°, 53.6°, and 57.1° matched well with the [220], [311], [222], [400], [422], and [511] planes of Fe_3O_4 crystals. The crystal structure data were in close agreement with the reported data and can be assigned to the magnetite phase of iron oxide.[46] The average diameter was calculated according to the Debye–Scherrer equation, which was in accordance with the SPR peak data of raw SPIONs. The composition of the SPIONs recovered from the Rutherford backscattering spectroscopy analysis (Figure 2B; Table S2) and energy-dispersive X-ray spectroscopy (Figure S3) study confirmed the presence of Fe and O, indicating the presence of the magnetite form Fe_3O_4.

Diffuse reflectance spectroscopy

Bandgap analysis was undertaken to test their light response in the visible region and to detect any capability toward PDT.[47] The DRS of SPIONs shows the characteristic absorbance in the range of 300–700 nm (Figure 2C). OP-SPIONs and PP-SPIONs showed high reflectance, while AP-SPIONs and LP-SPIONs showed comparatively low reflectance and high absorption. By utilizing the percentage reflectance, the bandgap energies were calculated and found to vary from 2.7 eV to 2.9 eV, indicating low-bandgap semiconductor properties (Figure 2D).[48]

Photoluminescence spectroscopy

The photoluminescence of the synthesized SPIONs was also determined. Owing to the emission of natural compounds present in the peel extracts, the spectrum was difficult to analyze; however, upon excitation at λ_{ex} =270 nm, the synthesized LP-SPIONs and OP-SPIONs exhibited a strong green emission band at λ_{em} =546 nm. The major peak is further red-shifted to λ_{em} =574 nm in PP-SPIONS and

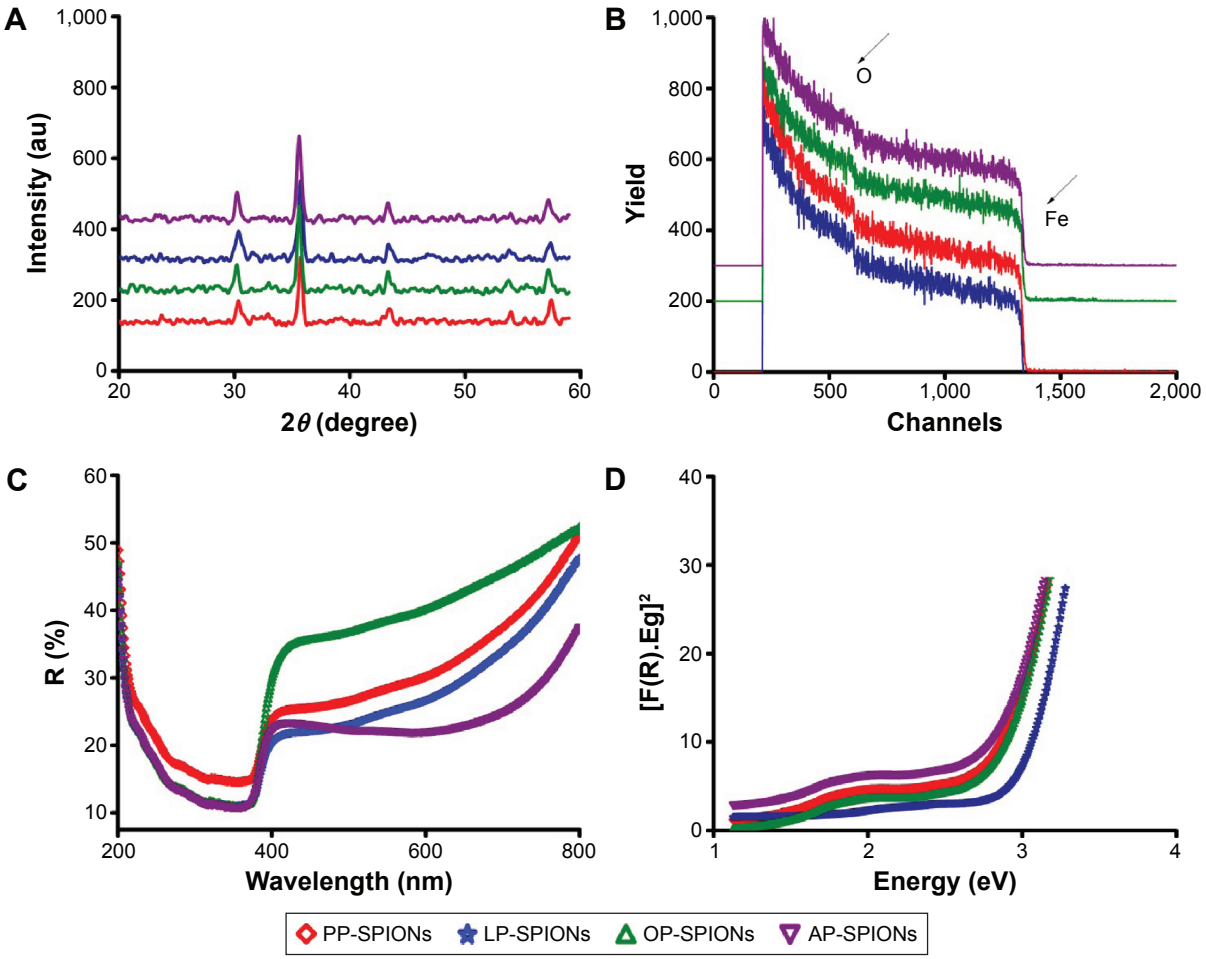

Figure 2 Structural and optical characterization of SPIONs.
Notes: (**A**) XRD patterns of the samples, (**B**) Rutherford backscattering spectra, and (**C**, **D**) diffuse reflectance spectra showing the composition and bandgap energies of the synthesized bio-SPIONs.
Abbreviations: AP-SPIONs, apple peel-mediated SPIONs; LP-SPIONs, lemon peel-mediated SPIONs; OP-SPIONs, orange peel-mediated SPIONs; PP-SPIONs, pomegranate peel-mediated SPIONs; SPIONs, superparamagnetic iron oxide nanoparticles; XRD, X-ray diffraction.

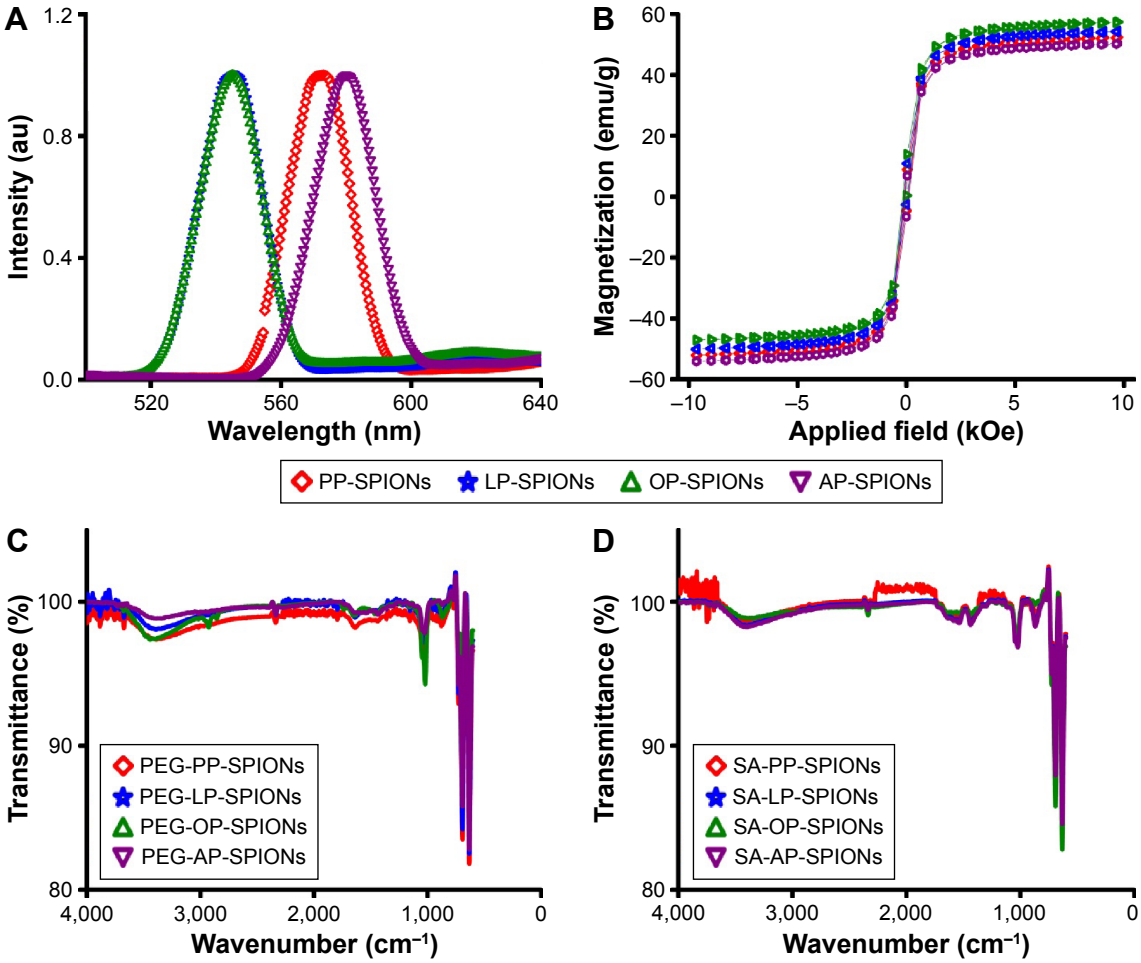

Figure 3 Fluorescence spectra, magnetization response and FTIR spectra.
Notes: (**A**) Fluorescence emission spectra where λ_{ex} =270 nm and (**B**) magnetization curve of bio-SPIONs. FTIR spectra of (**C**) PEG-SPIONs and (**D**) SA-SPIONs functionalized through MW incubation.
Abbreviations: AP-SPIONs, apple peel-mediated SPIONs; FTIR, fourier transform infrared; LP-SPIONs, lemon peel-mediated SPIONs; MW, microwave; OP-SPIONs, orange peel-mediated SPIONs; PEG, polyethylene glycol; PP-SPIONs, pomegranate peel-mediated SPIONs; SA, succinic anhydride; SPIONs, superparamagnetic iron oxide nanoparticles.

λ_{em} =580 nm in LP-SPIONs (Figure 3A), which is attributed to the radiative recombination of mobile electrons on the octahedral site. The presence of natural compounds in peel extracts could serve to explain the red shift seen in the emission spectra as they may be somewhat bulky and complex. Typical emissions reported in literature range from 465 nm to 550 nm and vary drastically depending on the size of the SPIONs studied and their capping agents.[27,49–51] It is inferred from the optical properties that the synthesized SPIONs may have potential application in visible-light driven PDT for treating cancers.

The magnetic study of bio-SPIONs shows no sizable hysteresis in OP-SPIONs, PP-SPIONs, AP-SPIONs, and LP-SPIONs (Figure 3B) at room temperature. Thus, bio-SPIONs possess superparamagnetism and are capable of altering proton relaxation in the tissue microenvironment, leading to T2 mode of MRI contrast enhancement.

Surface modification with bidentate linkers

One-pot surface engineering of SPIONs was devised with the bidentate linkers PEG or SA to find their suitability for developing multifunctional linkers, encapsulation of drugs, and targeting opportunities in developing theranostics for clinical application. The bonding status of the linkers on the surface of the NPs was confirmed by FTIR spectrometry and FESEM.

FTIR analysis of PEG-SPIONs and SA-SPIONs

FTIR analysis of prepared peel extracts and SPIONs indicated the presence of phytochemicals on the NP surface (Figures S4 and S5). The broad stretching vibrations at 3,000–3,700 cm^{-1} confirm the presence of polyhydroxyl

compounds. However, broad but weak stretching in the range of 1,350–1,700 cm^{-1} indicates the presence of unsaturation and the presence of –C=O groups on the surface of SPIONs.[48] Decrease in intensity of these two principal peaks in the SPIONs as compared to the peel extracts indicates that phytochemicals have played their role in stabilizing the SPION surface. The corresponding adsorption frequencies at low wave numbers (<700 cm^{-1}) come from vibrations of the Fe–O bonds of iron oxide, indicating Fe–O stretching vibration and Fe–O–Fe stretching in all NPs.[52–55] The presence of strong Fe–O–Fe stretching peak comments on the presence of Fe_3O_4.[56] The presence of multifunctional organic compounds on the surface of iron oxide NPs could enhance the hydrophilicity, which is favorable for applications in aqueous solutions and for preventing aggregation of SPIONs or uncontrolled growth.

Moreover, use of SA as a linker on the NP surface results in two prominent carboxyl peaks in FTIR analysis, confirming the conjugation of SA onto the NP surface (Figure 3C and D), whereas broad carbonyl and broad hydroxyl acid peaks indicate that the carboxylic acid functionality has coordinated with the NP surface for stabilization. Similarly, FTIR analysis of PEG-modified NPs displayed weak OH stretching as the hydroxyl is involved in binding onto the NP surfaces. A very weak carbonyl stretch in both indicates that a small amount of the phytochemicals in the orange and pomegranate peel extracts is still present on the NP surface. The FTIR spectroscopic results of all experiments give qualitative confirmation of SPION synthesis via MW irradiation and coating. Furthermore, the synthesized SPIONs were in the form of stable colloidal solutions showing a uniform distribution and no aggregation between the particles. This also confirms the role of the phytochemical covering on the surface of the SPIONs.[56]

FESEM and AFM images of PEG-SPIONs and SA-SPIONs

Low-resolution transmission electron micrographs of SPIONs (PEG-functionalized through MW incubation) were obtained on FESEM. Results revealed that the particles were regular in size and shape and showed no aggregation; however, a few flakes were detected as well. FESEM analysis shows that the functionalized PEG-PP-SPIONs and PEG-OP-SPIONs are roughly dumbbell shaped, whereas PEG-LP-SPIONs and PEG-AP-SPIONs are more circular in morphology (Figure 4).

AFM analysis of SPIONs (SA-functionalized) showed that the functionalized SPIONs are roughly circular in nature (Figure 5). The transparent shell of PEG and SA becomes slightly thicker in FESEM and AFM images, as PEGylation and carboxylation increased the size of NPs with narrow size distribution. While the largest functionalized NP was found with a diameter of 109±1.04 nm, the mean size of the functionalized SPIONs – as gathered from FESEM and AFM images – was 70.56±9.26 nm. Many functionalized SPIONs were created with diameters more than 60±1.03 nm; the vast majority (80.3%) had diameters ≤75±2.04 nm.

The complexity of the fruit peel extract utilized in this study may have significant effects on the deposition properties of the bio-SPIONs and may be an important driver in the NP size increment.

The hydrodynamic diameter of functionalized IONPs was found using dynamic light scattering (Zetasizer Nano-ZSP; Malvern Instruments). Table S3 shows the average hydrodynamic sizes of the PEG-SPIONS and the SA-SPIONs to be 78.25 nm and 60.46 nm, respectively. It is also evident from Table S3 that SA-SPIONs are smaller in size than PEG-SPIONs as SA forms a thin layer around the SPIONs.

Stability of SPIONs

The stability of NPs is a crucial criterion for their successful implementation in biomedical applications. Therefore, the in vitro stability of the biosynthesized and functionalized SPIONs was monitored by measuring the absorbance. SPION suspensions were placed in Milli-Q water and aqua sonicated for 1 hour. The samples were then placed in a cuvette, and absorbance was obtained at different intervals over a period of 2 months. Figure S6 and S7 compares the change over time for bio-SPIONs and functionalized SPIONs. All samples were found to be stable, displaying optimal stability.

MR relaxometry measurements

In order to investigate the potential usefulness of the prepared MRI contrast agent, relaxivity measurements were carried out. Samples of four different-sized SPIONs were prepared with different iron concentrations (determined by inductively coupled plasma atomic emission spectroscopy) in 3% agarose gel. We measured the R_2 values from the linear relationship of the transverse relaxation rates, $(1/T_2)$, versus the magnetic metal [Fe] concentrations. The inverse relaxation times $(1/T_2 = R_2)$ of SPIONs in water as a function of Fe concentration are shown in Figure 6.

To enhance the MR signal images, contrast agents must exhibit either accelerated spin–lattice relaxation (T_1), which leads to bright or positive contrast images, or increased spin–spin relaxation (T_2), which leads to dark or negative contrast images.

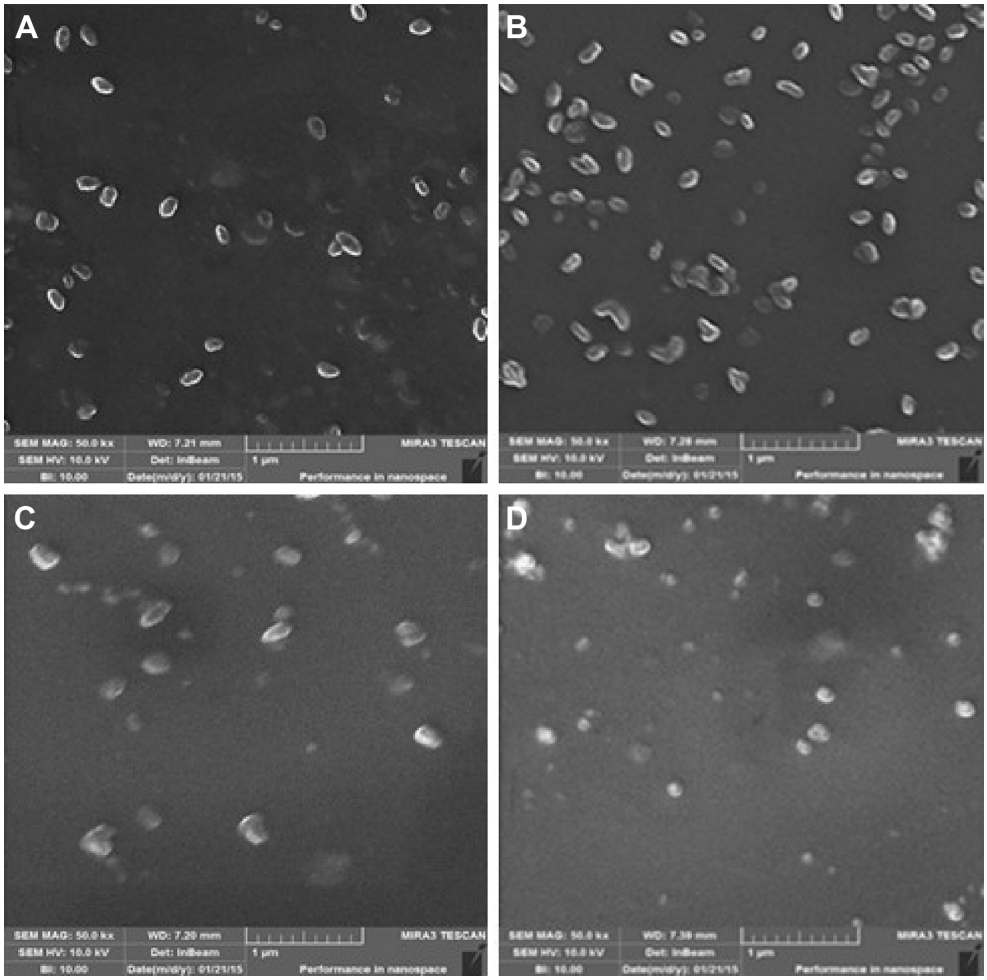

Figure 4 FESEM images of (**A**) PEG-PP-SPIONs, (**B**) PEG-LP-SPIONs, (**C**) PEG-LP-SPIONs, and (**D**) PEG-LP-IONPs functionalized through MW incubation.
Note: Transparent thin shell surrounding the NPs indicates successful PEGylation.
Abbreviations: FESEM, field emission scanning electron microscopy; IONP, iron oxide nanoparticles; LP-SPIONs, lemon peel-mediated SPIONs; MW, microwave; NPs, nanoparticles; PEG, polyethylene glycol; PP-SPIONs, pomegranate peel-mediated SPIONs; SPIONs, superparamagnetic iron oxide nanoparticles.

The ferrite NPs have a much larger magnetic moment than gadolinium ions (used as T_1 contrast agents) and produce larger magnetic field inhomogeneity. Due to this property of SPIONs, they are considered to be ideal T_2 contrast agents.[57]

Commercial Resovist has a core composition of magnetite–Fe_3O_4/maghemite–Fe_2O_3 coated with carboxydextran (R_1 =19.4±0.3 mM^{-1} s^{-1} and R_2 =185.8±9.3 mM^{-1} s^{-1}). The use of IONPs as T_2 contrast agent originates from the large hydrodynamic diameter of many clinically applied products or agglomeration of individual NPs. The impact of surface functionalization and compartmentalization of NPs on contrast enhancement has been reported recently.[58] Moreover, by surface modification, the same SPIONs could also be applied for T_1-weighted imaging, optimizing the imaging parameters. Therefore, the surface chemistry is important for controlling the hydrodynamic size for MRI contrast enhancement and internalization of SPIONs.

The magnetic properties of PEG-functionalized SPIONs were compared with those of same-gradient Fe of equivalent concentration. PP-SPIONs (82±5.04 nm) showed the highest relaxation enhancement, with R_2 value of 225 mM^{-1} s^{-1} at 1.5 T. This is because of the comparatively large size and high magnetization saturation. For LP-SPIONs (70±3.21 nm), OP-SPIONs (65±2.0 nm), and AP-SPIONs (56±8.09 nm), the R_2 values decrease to 202 mM^{-1} s^{-1}, 155 mM^{-1} s^{-1}, and 146 mM^{-1} s^{-1}, respectively (Figure 6C). According to the quantum mechanical outer sphere theory, the T_2 relaxivity or the spin–spin relaxation is highly dependent on the saturation magnetization of the NPs.[57] Greater T_2 relaxivity is due to the fact that larger NPs with higher saturation magnetization can afford more effective magnetic relaxations to water protons around the

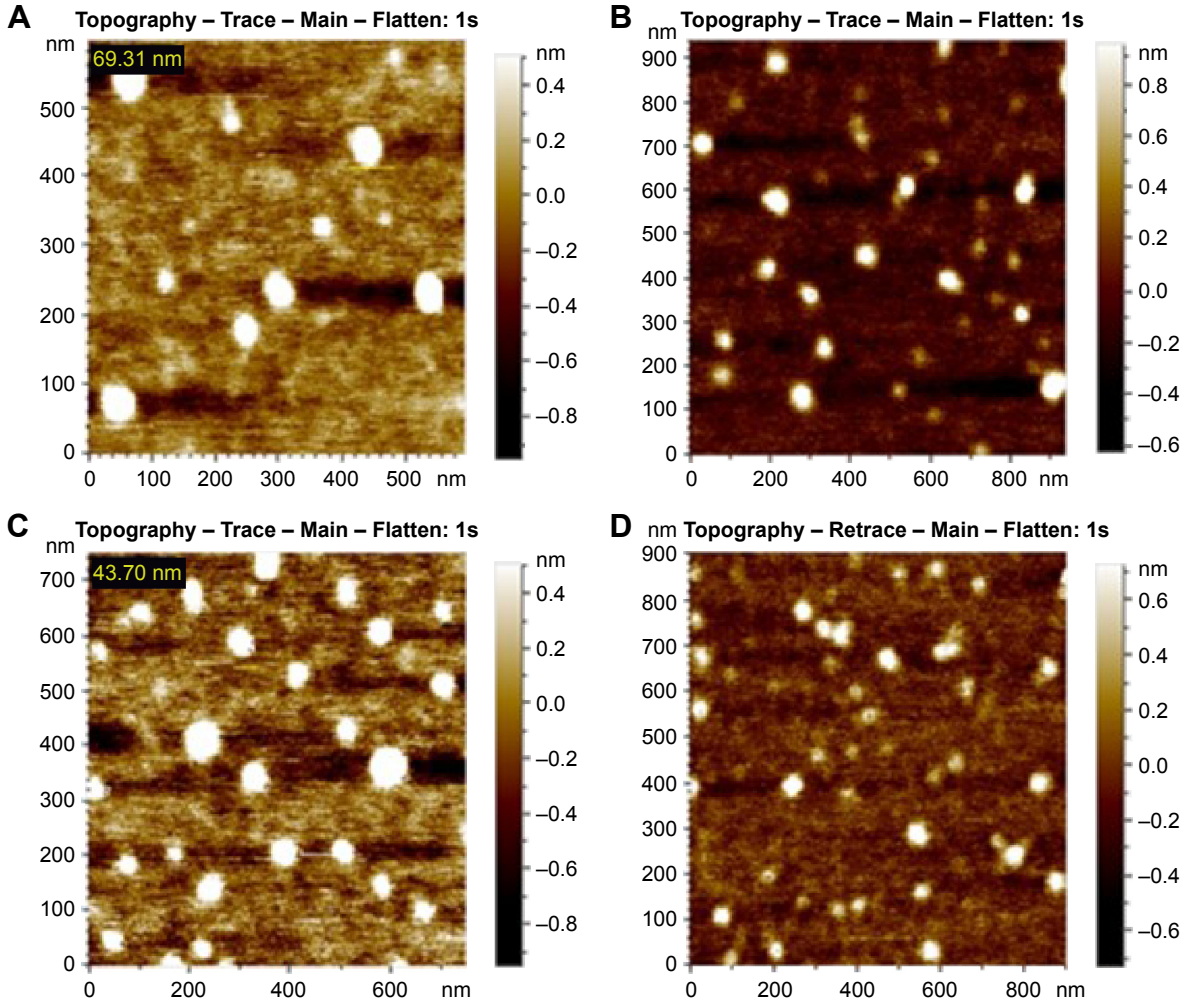

Figure 5 AFM images of (**A**) SA-PP-SPIONs, (**B**) SA-OP-SPIONs, (**C**) SA-AP-SPIONs, and (**D**) SA-LP-SPIONs functionalized through MW incubation.
Abbreviations: AFM, atomic force microscopy; AP-SPIONs, apple peel-mediated SPIONs; LP-SPIONs, lemon peel-mediated SPIONs; MW, microwave; OP-SPIONs, orange peel-mediated SPIONs; PP-SPIONs, pomegranate peel-mediated SPIONs; SA, succinic anhydride; SPIONs, superparamagnetic iron oxide nanoparticles.

NPs. Contrast effects of NPs are highly size dependent. By controlling the size, we can achieve much higher contrast enhancement as the R_2 values of SPIONs at 1.5 T were much higher than those of the commercial SPION Resovist (Figure 6).

Effects of SPIONs, PEG-SPIONs, and SA-SPIONs on the integrity of red blood cells

Figure 7A shows the hemolytic index (in percentage) of the biosynthesized nonfunctionalized SPIONs. Almost no hemoglobin leakage was found in any sample, implying nil cell lysis. Hemolytic studies were conducted following the standard protocol (American Society for Testing and Materials [ASTM] F756-00), and the hemolytic index of all SPIONs was found to be well below the standard (5%), showing their highly nonhemolytic nature.

Cell viability studies

To evaluate the cytotoxicity of SPIONs, treated cells were incubated in the dark and subsequently evaluated by the SRB assay. As shown in Figure 7B, all the surviving fractions of the treated HeLa cells had, on the average, values >90% at all the concentrations used (0–150 µg/mL). As these results indicated, the cytotoxicity values of SPIONs were quite low, with no significant influence of the concentrations on the cytotoxicity.

The cytotoxicity with different surface functionalizations was further confirmed to investigate the effect of surface modifications (Figure 7C and D, as well as Figure S8). The results show that bioreduced SPIONs were most favorable for cell growth and displayed no toxicity even at high concentrations of 150 µg/mL. They remained nontoxic even after the functionalization procedure. It is evident from the results that these particles were successfully functionalized

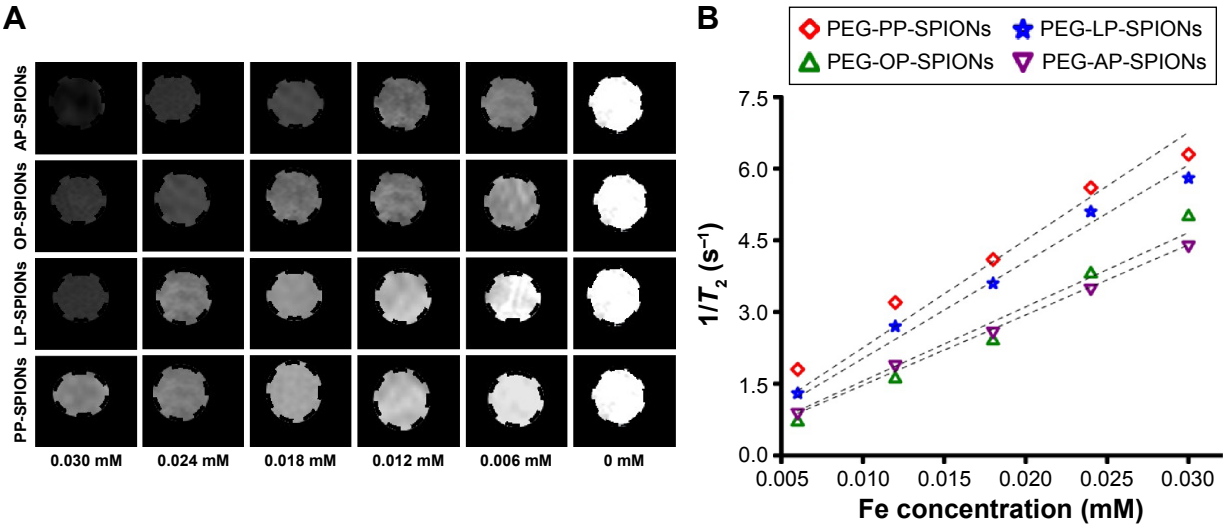

C

S No	Formulation	Crystallite size (nm)	Mean size after functionalization (nm)	R_2 ($mM^{-1}s^{-1}$)
1	PEG-PP-SPIONs	28.7±0.23	82±5.04	225
2	PEG-LP-SPIONs	25.5±0.35	70±3.21	202
3	PEG-OP-SPIONs	22.2±0.05	65±2.0	155
4	PEG-AP-SPIONs	17.0±0.43	56±8.09	146
5	Resovist®			185

Figure 6 MR studies of SPIONs.
Notes: (**A**) T_2-weighted images of cell suspensions with different metal ion (Fe in millimoles) concentrations at 1.5 T. (**B**) Linear fitting of $1/T_2$ as a function of Fe concentration. (**C**) MR transverse relaxivity (R_2) values of PEG-SPIONs functionalized through MW incubation.
Abbreviations: AP-SPIONs, apple peel-mediated SPIONs; LP-SPIONs, lemon peel-mediated SPIONs; MR, magnetic resonance; MW, microwave; OP-SPIONs, orange peel-mediated SPIONs; PEG, polyethylene glycol; PP-SPIONs, pomegranate peel-mediated SPIONs; SPIONs, superparamagnetic iron oxide nanoparticles.

through simple MW incubation. The MW incubation method was quick compared to conventional surface functionalization, which involves long heating time. Both batches of functionalized SPIONs with PEG and SA linkers displayed very minimal toxicity, suggesting their favorable behavior for use in cancer theranostic development.

This study reveals the effects of three types of SPIONs on HeLa cells and provides significant insight into the possible mechanism through which they exert their toxic effects on these cells. Quantitative SRB assay data (Figure 7B) showed no significant statistical difference ($P>0.05$) in terms of viability of treated versus NTCs up to the highest concentration of 150 µg/mL. Compared with the functionalized batches of SPIONs, the nonfunctionalized batch consistently exhibited lower cytotoxicity. The use of green and more biogenic synthesis route thus increased the overall safety, circumventing the need of any functionalization prior to biological applications.

The development of multifunctional nanomaterials with minimal cytotoxicity is highly desired. PEG and SA are very suitable for use as coating materials for SPIONs. Such coated particles would have great potential to be used as delivery agents for anticancer drugs, DNA, and proteins due to their large surface area, tunable size, and well-defined surface properties.

Although the surface modifications via carboxylation or PEGylation appear to significantly shield the surface of the particles, this does not lead to appreciable decrease in cytocompatibility even at a concentration up to 150 µg/mL (Figure 7).

Photodestruction of HeLa cells

Photodestruction of HeLa cells in the presence of bio-SPIONs was assessed by the MTT assay. After irradiation, they induced significant cytotoxicity to the HeLa cells in a dose-dependent manner.

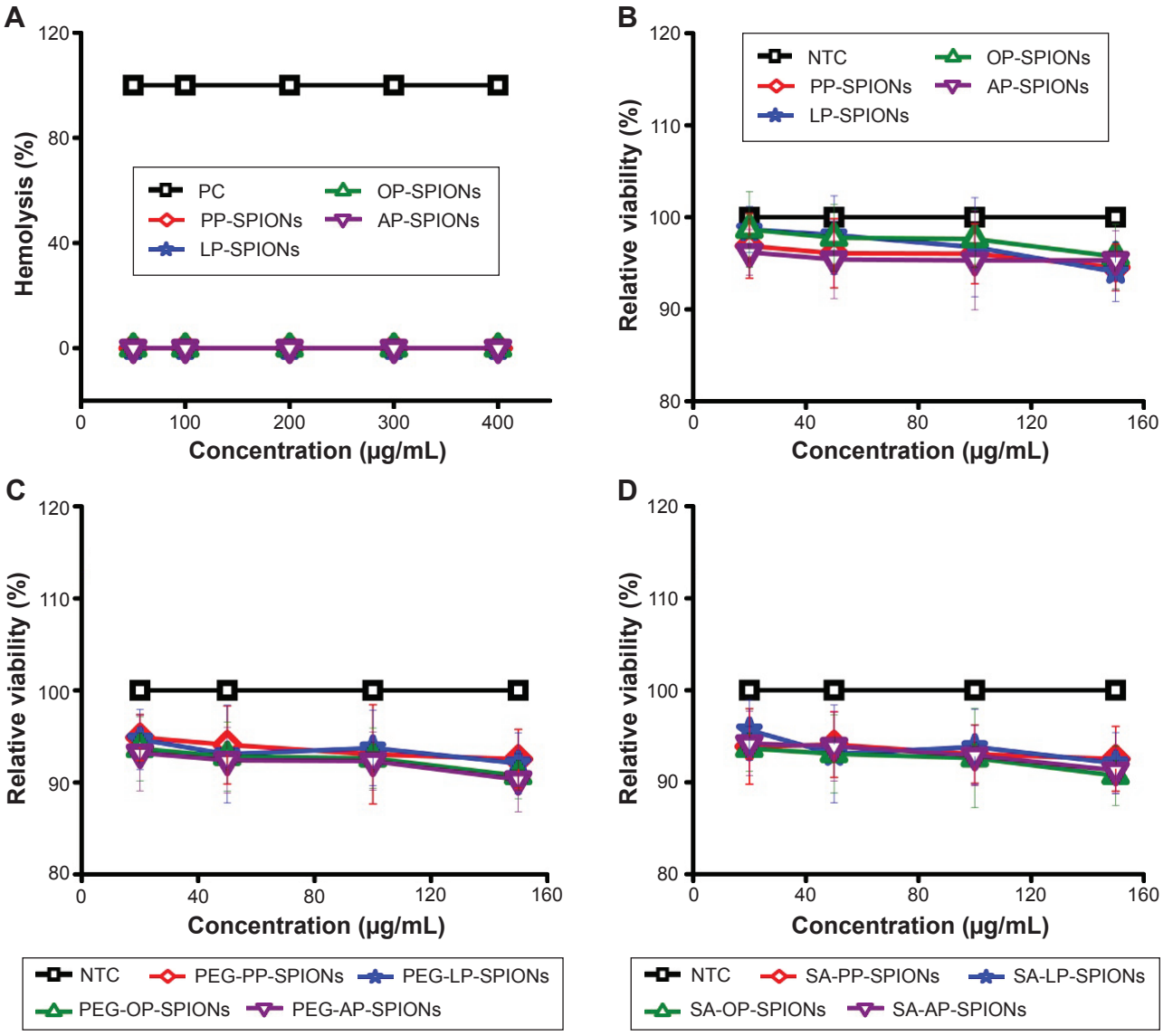

Figure 7 Biocompatibility of SPIONs.

Notes: (**A**) Hemolysis results of bio-SPIONs. Relative cell viability curves of (**B**) bio-SPIONs, (**C**) PEG-SPIONs, and (**D**) SA-SPIONs functionalized through MW incubation. Percentage viabilities (mean ± SD) were calculated ($P<0.05$; two-tailed *t*-test).

Abbreviations: AP-SPIONs, apple peel-mediated SPIONs; LP-SPIONs, lemon peel-mediated SPIONs; OP-SPIONs, orange peel-mediated SPIONs; NTC, nontreated cell; PP-SPIONs, pomegranate peel-mediated SPIONs; PEG, polyethylene glycol; SA, succinic anhydride; SPIONs, superparamagnetic iron oxide nanoparticles; SD, standard deviation; PC, positive control.

As demonstrated in Figure 8A, cells treated with SPIONs were killed more effectively when compared with the control. The photokilling effects of PP-SPIONs, LP-SPIONs, OP-SPIONs, and AP-SPIONs were quite similar, although their absorption spectra showed some difference. It is also demonstrated (Figure 8A) that the survival fractions decreased with increasing NP concentrations. It decreased to 23% for the cells treated with OP-SPIONs at a concentration of 150 μg/mL and may be useful against different cancers as a photosensitizer for PDT.

At 100 μg/mL, a differential effect of all the SPIONs was observed, which increased with increasing concentration. At a concentration of 150 μg/mL, all samples exhibited a strong differential activity against the cancer cells, as compared to the NTCs, with percentage viability values of 33.42±3.50 μg/mL, 27.02±6.36 μg/mL, 24.57±4.50 μg/mL, and 25.85±3.36 μg/mL for PP-, LP-, OP-, and AP-SPIONs, respectively. Hence, this concentration was considered as optimal for the cultures.

Furthermore, the ratio of CV of HeLa cells after light irradiation to that of cells without light irradiation (CV+/CV−) is shown in Figure 8B. Smaller CV+/CV− ratios at any concentration suggest that SPIONs can induce significant phototoxicity against HeLa cells.

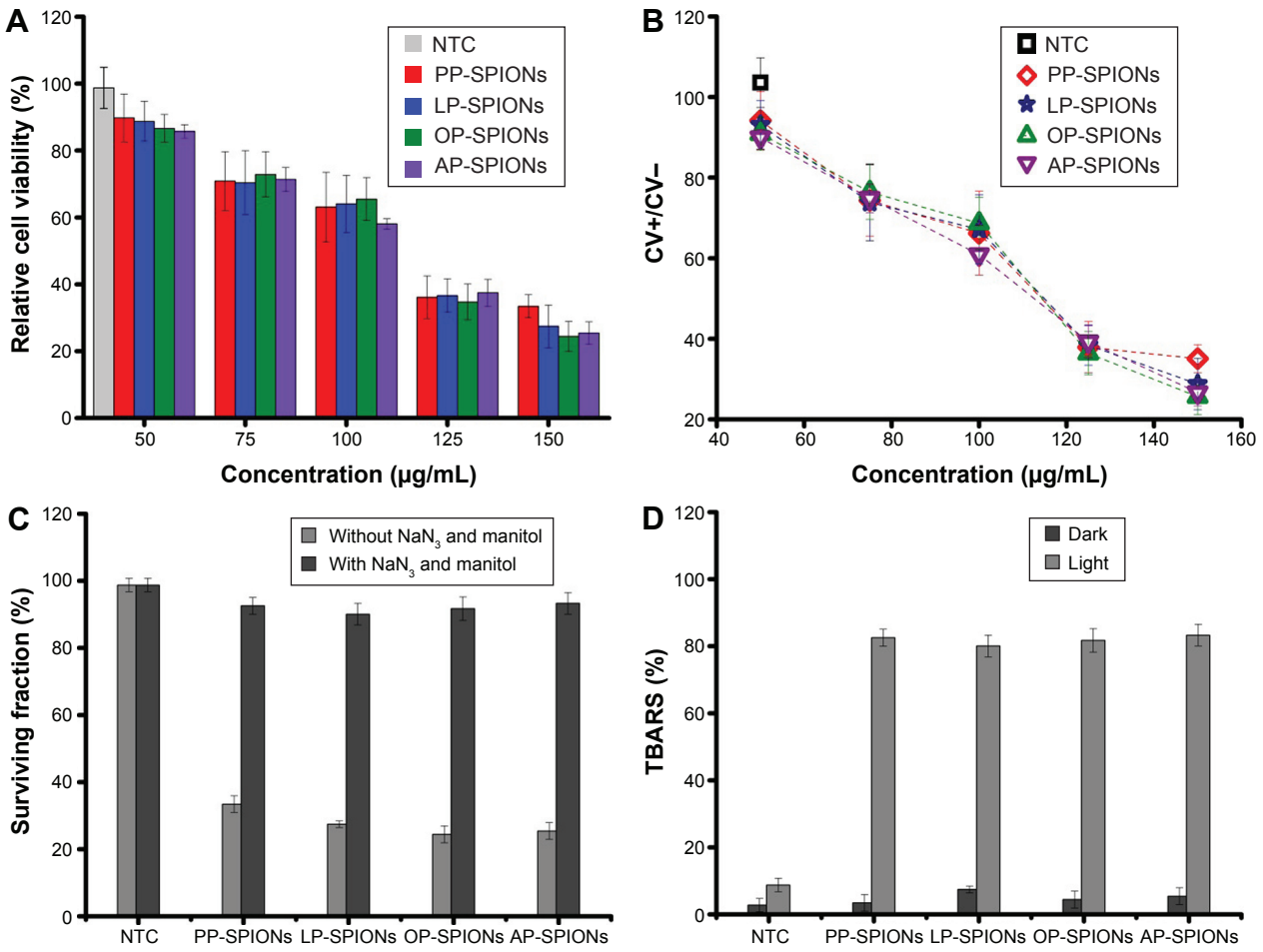

Figure 8 Photo-toxicity studies.

Notes: (**A**) PDT effects of bio-SPIONs on HeLa cell viability. (**B**) Cell viability ratios in light and dark reactions (CV+/CV–) vs concentration. (**C**) Changes in the surviving fractions of the treated HeLa cells preincubated with and without the scavengers (NaN_3 and mannitol). (**D**) TBA assay results for SPION exposure. Data are expressed as percentage (mean ± SD) relative to the NTC sample ($P<0.05$; two-tailed *t*-test).

Abbreviations: AP-SPIONs, apple peel-mediated SPIONs; CV, cell viability; HeLa, human cervical epithelial malignant carcinoma; LP-SPIONs, lemon peel-mediated SPIONs; NTC, nontreated cell; OP-SPIONs, orange peel-mediated SPIONs; PDT, photodynamic therapy; PP-SPIONs, pomegranate peel-mediated SPIONs; SPION, superparamagnetic iron oxide nanoparticle; TBA, thiobarbituric acid; TBARS, TBA-reactive substances; SD, standard deviation.

It is known that the PDT effect is often limited by the high hydrophilicity of the photosensitizer.[59] Water-soluble bio-SPIONs synthesized via the green method demonstrated their ability to produce high amounts of ROS under light exposure, unveiling the PDT effect of such particles.

Temperature measurements of SPIONs undergoing irradiation were carried out in water containing 10% FBS, in the absence of HeLa cells, at different concentrations (Supplementary materials). The results were assessed after each minute by exposing them to light. The samples showed a small increase in temperature at 1 mg/mL from 0.2°C to 0.4°C (Table S4). The temperature increased from 1.3°C to 1.8°C when 5 mg/mL of each sample was added to water and from 2.8°C to 3.1°C when 10 mg/mL of each sample was added to water. Thus, this eliminated the involvement of hyperthermia in the photokilling of HeLa cells.

ROS quantification

The mechanism of the photokilling effect on cancer cells is very complex. It has been identified that photoexcited NPs in aqueous solution result in the formation of various ROS, such as hydroxyl radicals (·OH), hydrogen peroxide (H_2O_2), superoxide radicals ($\cdot O_2^-$), and singlet oxygen ($^1O_2$). ROS target the cancer cells and finally lead to cell death.

In order to study the function of ROS in the photokilling effect, HeLa cells were preincubated with and without NaN_3, a scavenger of $^1O_2$, and mannitol, a scavenger of hydroxyl radical (HO•). Pretreatment of HeLa by NaN_3 and mannitol indeed dramatically suppressed the ROS levels. In the presence of these scavengers, the surviving fractions of the cells treated with SPIONs at a concentration of 150 μg/mL increased evidently (Figure 8C). The decrease in CV after light exposure (tungsten source, 100 W, 5 minutes), as compared to unexposed samples, and an increased survival rate

when experiments were performed with ROS scavengers showed that PDT might be a possible mechanism behind the photokilling of HeLa Cells.

TBA-reactive substances assay

LPO level was estimated by the TBA reaction to investigate the induction of oxidative stress by the bio-SPIONs. This method was used to spectrophotometrically measure the color produced by the reaction of TBA with MDA at 532 nm. TBA-reactive substances are formed as a by-product of LPO (ie, as degradation products of fats), which can be detected using TBA as a reagent. LPO level can be observed by measuring the formation of MDA, one of the products of membrane LPO.

The average MDA level in light-and dark-exposed samples is shown in Figure 8D. For HeLa cells, the average MDA level in NTCs was 8.05±3.73 and 4.16±3.23 in light- and dark-exposed samples, respectively. Bio-SPION treatment resulted in at least tenfold increase in TBA-reactive substances concentration compared with NTCs. A significant ($P \leq 0.05$) induction of MDA was obtained in HeLa under light exposure as compared to the samples maintained under dark, clearly indicating that bio-SPIONs were responsible for the ROS-assisted photokilling of HeLa cells.

Conclusion

SPIONs were successfully synthesized and functionalized utilizing MW-assisted green approach. The fruit peel extracts acted as reducing and capping agents, rendering the whole procedure cost-effective and environment friendly. The bio-SPIONs were found to be water soluble, with promising hemocompatibility at a concentration as high as 400 µg/mL. The bio-SPIONs were capable of active photokilling of HeLa cells, which showed 23% decreased survival, and relatively high MR imaging potential, with R_2 value of 225 mM^{-1} s^{-1}. The formation of SPIONs using environmentally benign reagents in minimal time paves the way for entrapment of therapeutic molecules, fluorescent agents, and targeting ligands without risking interference from potentially toxic reagents and capping agents.

Acknowledgments

The authors are grateful to Dr Mustansar Mahmood Waraich, Professor, and magnetic resonance imaging technologists at the Diagnostic Radiology Department of Quaid-e-Azam Medical College Bahawalpur Victoria Hospital for their cooperation and technical support. Special thanks to Abdul Haleem, PhD student, Department of Microbiology, Quaid-e- Azam University, and Mr Naeem (NCP) for UV-vis and FTIR instrumentation time and assistance. Ms Shazia Bano thanks the Higher Education Commission for the Indigenous Fellowship to support her PhD studies.

Disclosure

The authors report no conflicts of interest in this work.

References

1. Rosen JE, Chan L, Shieh D-B, Gu FX. Iron oxide nanoparticles for targeted cancer imaging and diagnostics. *Nanomedicine*. 2011;8(3):275–290.
2. Hao H, Ma Q, He F, Yao P. Doxorubicin and Fe3O4 loaded albumin nanoparticles with folic acid modified dextran surface for tumor diagnosis and therapy. *J Mater Chem B*. 2014;2(45):7978–7987.
3. Quinto CA, Mohindra P, Tong S, Bao G. Multifunctional superparamagnetic iron oxide nanoparticles for combined chemotherapy and hyperthermia cancer treatment. *Nanoscale*. 2015;7(29):12728–12736.
4. Kossatz S, Grandke J, Couleaud P, et al. Efficient treatment of breast cancer xenografts with multifunctionalized iron oxide nanoparticles combining magnetic hyperthermia and anti-cancer drug delivery. *Breast Cancer Res*. 2015;17:66.
5. Xuan S-H, Lee S-F, Lau JT-F, et al. Photocytotoxicity and magnetic relaxivity responses of dual-porous Î[3]-Fe2O3@meso-SiO2 microspheres. *ACS Appl Mater Interfaces*. 2012;4(4):2033–2040.
6. Cheng L, Yang K, Li Y, et al. Facile preparation of multifunctional upconversion nanoprobes for multimodal imaging and dual-targeted photothermal therapy. *Angew Chem Int Ed Engl*. 2011;50(32):7385–7390.
7. Aggarwal P, Hall JB, McLeland CB, Dobrovolskaia MA, McNeil SE. Nanoparticle interaction with plasma proteins as it relates to particle biodistribution, biocompatibility and therapeutic efficacy. *Adv Drug Deliv Rev*. 2009;61(6):428–437.
8. Benelli G. Plant-mediated biosynthesis of nanoparticles as an emerging tool against mosquitoes of medical and veterinary importance: a review. *Parasitol Res*. 2016;115(1):23–34.
9. Jain N, Bhargava A, Majumdar S, Tarafdar JC, Panwar J. Extracellular biosynthesis and characterization of silver nanoparticles using *Aspergillus flavus* NJP08: a mechanism perspective. *Nanoscale*. 2011;3(2):635–641.
10. Badhani B, Sharma N, Kakkar R. Gallic acid: a versatile antioxidant with promising therapeutic and industrial applications. *RSC Adv*. 2015;5(35):27540–27557.
11. Huang G, Li H, Chen J, et al. Tunable T1 and T2 contrast abilities of manganese-engineered iron oxide nanoparticles through size control. *Nanoscale*. 2014;6(17):10404–10412.
12. Im GH, Kim SM, Lee D-G, Lee WJ, Lee JH, Lee IS. Fe3O4/MnO hybrid nanocrystals as a dual contrast agent for both T1- and T2-weighted liver MRI. *Biomaterials*. 2013;34(8):2069–2076.
13. Peeples B, Goornavar V, Peeples C, et al. Structural, stability, magnetic, and toxicity studies of nanocrystalline iron oxide and cobalt ferrites for biomedical applications. *J Nanopart Res*. 2014;16(2):1–10.
14. Oberdörster G. Safety assessment for nanotechnology and nanomedicine: concepts of nanotoxicology. *J Intern Med*. 2010;267(1):89–105.
15. Clift MJ, Rothen-Rutishauser B, Brown DM, et al. The impact of different nanoparticle surface chemistry and size on uptake and toxicity in a murine macrophage cell line. *Toxicol Appl Pharmacol*. 2008;232(3):418–427.
16. Rothen-Rutishauser B, Mühlfeld C, Blank F, Musso C, Gehr P. Translocation of particles and inflammatory responses after exposure to fine particles and nanoparticles in an epithelial airway model. *Part Fibre Toxicol*. 2007;4(1):1–9.
17. Yacobi NR, Phuleria HC, Demaio L, et al. Nanoparticle effects on rat alveolar epithelial cell monolayer barrier properties. *Toxicol In Vitro*. 2007;21(8):1373–1381.
18. Ai J, Biazar E, Jafarpour M, et al. Nanotoxicology and nanoparticle safety in biomedical designs. *Int J Nanomedicine*. 2011;6:1117–1127.

19. Muhlfeld C, Gehr P, Rothen-Rutishauser B. Translocation and cellular entering mechanisms of nanoparticles in the respiratory tract. *Swiss Med Wkly*. 2008;138(27–28):387–391.
20. Namvar F, Rahman HS, Mohamad R, et al. Cytotoxic effect of magnetic iron oxide nanoparticles synthesized via seaweed aqueous extract. *Int J Nanomedicine*. 2014;9:2479–2488.
21. Nadagouda MN, Castle AB, Murdock RC, Hussain SM, Varma RS. In vitro biocompatibility of nanoscale zerovalent iron particles (NZVI) synthesized using tea polyphenols. *Green Chem*. 2010;12(1):114–122.
22. Mahdavi M, Namvar F, Ahmed MB, Mohamad R. Green synthesis and characterization of magnetic iron oxide (Fe_3O_4) nanoparticles using seaweed (*Sargassum muticum*) aqueous extract. *Molecules*. 2013; 18(5):5954–5964.
23. Shirazi H, Daneshpour M, Kashanian S, Omidfar K. Synthesis, characterization and in vitro biocompatibility study of Au/TMC/Fe3O4 nanocomposites as a promising, nontoxic system for biomedical applications. *Beilstein J Nanotechnol*. 2015;6:1677–1689.
24. Wu W, He Q, Jiang C. Magnetic iron oxide nanoparticles: synthesis and surface functionalization strategies. *Nanoscale Res Lett*. 2008;3(11):397–415.
25. Lopez-Tellez G, Balderas-Hernandez P, Barrera-Diaz CE, Vilchis-Nestor AR, Roa-Morales G, Bilyeu B. Green method to form iron oxide nanorods in orange peels for chromium(VI) reduction. *J Nanosci Nanotechnol*. 2013;13(3):2354–2361.
26. Dai J, Mumper RJ. Plant phenolics: extraction, analysis and their antioxidant and anticancer properties. *Molecules*. 2010;15(10): 7313–7352.
27. Bennet D, Kang SC, Gang J, Kim S. Photoprotective effects of apple peel nanoparticles. *Int J Nanomedicine*. 2014;9:93–108.
28. Sparr Eskilsson C, Björklund E. Analytical-scale microwave-assisted extraction. *J Chromatogr A*. 2000;902(1):227–250.
29. Kahrilas GA, Wally LM, Fredrick SJ, Hiskey M, Prieto AL, Owens JE. Microwave-assisted green synthesis of silver nanoparticles using orange peel extract. *ACS Sustain Chem Eng*. 2014;2(3):367–376.
30. Hu B, Wang S-B, Wang K, Zhang M, Yu S-H. Microwave-assisted rapid facile "green" synthesis of uniform silver nanoparticles: self-assembly into multilayered films and their optical properties. *J Phys Chem C*. 2008;112(30):11169–11174.
31. Grisaru H, Palchik O, Gedanken A, Palchik V, Slifkin MA, Weiss AM. Microwave-assisted polyol synthesis of CuInTe2 and CuInSe2 nanoparticles. *Inorg Chem*. 2003;42(22):7148–7155.
32. Horikoshi S, Abe H, Torigoe K, Abe M, Serpone N. Access to small size distributions of nanoparticles by microwave-assisted synthesis. Formation of Ag nanoparticles in aqueous carboxymethylcellulose solutions in batch and continuous-flow reactors. *Nanoscale*. 2010; 2(8):1441–1447.
33. Kobayashi H, Watanabe R, Choyke PL. Improving conventional enhanced permeability and retention (EPR) effects; what is the appropriate target? *Theranostics*. 2014;4(1):81–89.
34. Doane TL, Burda C. The unique role of nanoparticles in nanomedicine: imaging, drug delivery and therapy. *Chem Soc Rev*. 2012; 41(7):2885–2911.
35. Cai H, An X, Cui J, et al. Facile hydrothermal synthesis and surface functionalization of polyethyleneimine-coated iron oxide nanoparticles for biomedical applications. *ACS Appl Mater Interfaces*. 2013; 5(5):1722–1731.
36. Vichai V, Kirtikara K. Sulforhodamine B colorimetric assay for cytotoxicity screening. *Nat Protoc*. 2006;1(3):1112–1116.
37. Wang T, Jin X, Chen Z, Megharaj M, Naidu R. Green synthesis of Fe nanoparticles using eucalyptus leaf extracts for treatment of eutrophic wastewater. *Sci Total Environ*. 2013;466–467:210–213.
38. Shankar SS, Rai A, Ahmad A, Sastry M. Rapid synthesis of Au, Ag, and bimetallic Au core-Ag shell nanoparticles using Neem (*Azadirachta indica*) leaf broth. *J Colloid Interface Sci*. 2004;275(2):496–502.
39. Wang JH, Wang B, Liu Q, et al. Bimodal optical diagnostics of oral cancer based on Rose Bengal conjugated gold nanorod platform. *Biomaterials*. 2013;34(17):4274–4283.
40. Mahdavi M, Ahmad M, Haron M, et al. Synthesis, surface modification and characterisation of biocompatible magnetic iron oxide nanoparticles for biomedical applications. *Molecules*. 2013;18(7):7533–7548.
41. Chidambara Murthy KN, Jayaprakasha GK, Singh RP. Studies on antioxidant activity of pomegranate (*Punica granatum*) peel extract using in vivo models. *J Agric Food Chem*. 2002;50(17):4791–4795.
42. Fawole OA, Makunga NP, Opara UL. Antibacterial, antioxidant and tyrosinase-inhibition activities of pomegranate fruit peel methanolic extract. *BMC Complement Altern Med*. 2012;12:200.
43. Prasad D, Kunnaiah R. *Punica granatum*: a review on its potential role in treating periodontal disease. *J Indian Soc Periodontol*. 2014;18(4): 428–432.
44. Fateixa S, Nogueira HIS, Trindade T. Hybrid nanostructures for SERS: materials development and chemical detection. *Phys Chem Chem Phys*. 2015;17(33):21046–21071.
45. Saravanan P, Chandramohan G, Mariajancyrani J, Shanmugasundaram P. GC-MS analysis of phytochemical constituents in ethanolic bark extract of ficus religiosa linn. *Int J Pharm Pharm Sci*. 2011;6(1):457–460.
46. Yang H, Zhuang Y, Sun Y, et al. Targeted dual-contrast T1- and T2-weighted magnetic resonance imaging of tumors using multifunctional gadolinium-labeled superparamagnetic iron oxide nanoparticles. *Biomaterials*. 2011;32(20):4584–4593.
47. Zeferino RS, Flores MB, Pal U. Photoluminescence and Raman scattering in Ag-doped ZnO nanoparticles. *J Appl Phys*. 2011;109(1):014308.
48. Zhang H, Ji Z, Xia T, et al. Use of metal oxide nanoparticle band gap to develop a predictive paradigm for oxidative stress and acute pulmonary inflammation. *ACS Nano*. 2012;6(5):4349–4368.
49. Qu H, Ma H, Riviere A, Zhou W, O'Connor CJ. One-pot synthesis in polyamines for preparation of water-soluble magnetite nanoparticles with amine surface reactivity. *J Mater Chem*. 2012;22(8): 3311–3313.
50. Shi D, Sadat ME, Dunn AW, Mast DB. Photo-fluorescent and magnetic properties of iron oxide nanoparticles for biomedical applications. *Nanoscale*. 2015;7(18):8209–8232.
51. Atabaev T, Kim HK, Hwang YH. Fabrication of bifunctional core-shell Fe3O4 particles coated with ultrathin phosphor layer. *Nanoscale Res Lett*. 2013;8(1):357.
52. Sodipo BK, Aziz AA. A sonochemical approach to the direct surface functionalization of superparamagnetic iron oxide nanoparticles with (3-aminopropyl) triethoxysilane. *Beilstein J Nanotechnol*. 2015;5(1):1472–1476.
53. Yang R, An Y, Miao F, Li M, Liu P, Tang Q. Preparation of folic acid-conjugated, doxorubicin-loaded, magnetic bovine serum albumin nanospheres and their antitumor effects in vitro and in vivo. *Int J Nanomedicine*. 2014;9:4231–4243.
54. Kumar SR, Paulpandi M, ManivelRaja M, et al. An in vitro analysis of H1N1 viral inhibition using polymer coated superparamagnetic Fe3O4 nanoparticles. *RSC Adv*. 2014;4(26):13409–13418.
55. Santos ECS, dos Santos TC, Guimaraes RB, Ishida L, Freitas RS, Ronconi CM. Guanidine-functionalized Fe3O4 magnetic nanoparticles as basic recyclable catalysts for biodiesel production. *RSC Adv*. 2015;5(59):48031–48038.
56. Laurent S, Forge D, Port M, et al. Magnetic iron oxide nanoparticles: synthesis, stabilization, vectorization, physicochemical characterizations, and biological applications. *Chem Rev*. 2010;110(4):2574–2574.
57. Huang J, Zhong X, Wang L, Yang L, Mao H. Improving the magnetic resonance imaging contrast and detection methods with engineered magnetic nanoparticles. *Theranostics*. 2012;2(1):86–102.
58. Li R, Ji Z, Chang CH, et al. Surface interactions with compartmentalized cellular phosphates explain rare earth oxide nanoparticle hazard and provide opportunities for safer design. *ACS Nano*. 2014;8(2): 1771–1783.
59. Yao M, Gu C, Doyle FJ, Zhu H, Redmond RW, Kochevar IE. Why is Rose Bengal more phototoxic to fibroblasts in vitro than in vivo? *Photochem Photobiol*. 2014;90(2):297–305.